PHYSICAL REVIEW B VOLUME 38, NUMBER 16 1 DECEMBER 1988

Evolution of multilayer Ar and Ne films from two-dimensional to bulk behavior

Da-Ming Zhu and J. G. Dash
Department of Physics (FM-15), University of Washington, Seattle, Washington 98195

(Received 23 May 1988)

Argon and neon films on graphite have been studied in detail by high-resolution calorimetry, at temperatures from 60% of the bulk triple point (T_t) to several degrees above, and at coverages ranging from two to more than 20 molecular layers. Both adsorbates undergo a series of transformations, including layer formation, layer order-disorder transitions, individual layer melting, surface roughening, and surface melting. Layer transitions at thicknesses between two and six layers display Ising-like critical points, which evolve with increasing thickness to a broad roughening anomaly $T_R = 0.8T_t$. A distinct series of peaks extending from the region of ordering temperatures to temperatures above T_t is associated with the formation of each of the first four solid layers next to the substrate. Higher layers exhibit no individuality in their thermal behavior, and melting evolves into continuous surface melting. The thickness of the melt liquid at the surface of thick films corresponds to the predicted temperature dependence of surface melting in solids governed by dispersion forces. In thinner films the temperature dependence indicates short-range effective interactions, attributed to the intrusion of solid crystalline order into the liquid at the crystal-melt interface. A novel technique is developed for determining the profile of the crystal-melt interface, and applied to the Ar and Ne film systems. The profiles of both systems can be fitted by exponential or hyperbolic tangent functions. The experimental interface widths are found to be about six layers in Ne and four layers in Ar.

I. INTRODUCTION

Physisorbed films have attracted much experimental and theoretical interest in the past two decades. For much of this time, the focus has been on monolayer systems, but increasing attention is now being given to multilayer phenomena. Strong motivation for the work on thick films has been wetting phenomena[1] and the particular transition known as triple-point wetting.[2] Adsorbed multilayers are also useful as test systems for studies of some bulk surface properties, such as surface melting[3-10] and surface roughening.[11-28] Attention has been directed to the connections between film and bulk surface phenomena; for example, between layer critical points and the roughening temperature,[18,19,21] and between wetting, layer melting, and surface melting.[29,30] These topics are part of a global problem, the evolution from two-dimensional behavior to bulk characteristics as thickness increases from a single layer to macroscopic thickness.[31]

In order to explore these relationships, we carried out an extensive calorimetric study of Ar and Ne multilayer films adsorbed on graphite. Brief reports of some of the results of this study, principally the portions involving the thicker films, have been published,[7] but a complete account has not previously appeared. The experiment was primarily focused on surface melting and surface roughening in both systems, to study the evolution of these transitions with increasing coverage. Ar and Ne are particularly useful as model systems since their bulk[32] and monolayer phases[33,34] are known in considerable detail.

This paper is organized as follows. Section II describes the experimental details. In Sec. III the data are presented and described in general terms. Section IV contains a detailed analysis of the results associated with each of the principal regimes; discrete layer phenomena, roughening, and surface melting. The interpretation of the calorimetric study is consistent with the analysis of a neutron scattering investigation of the same system.[35] In Sec. V we construct a common phase diagram for the entire multilayer region, and discuss a number of questions that may be addressed in future work.

II. EXPERIMENTAL DETAILS

The calorimeter was the same as previously employed for monolayer studies[36] except for the adsorption cell and some minor changes. The cell, constructed specifically for the present studies, consists of a cylinder of exfoliated graphite foam tightly fitted into a thin walled copper chamber, 2 in. in diameter and 2 in. long. The graphite foam was heated to above 1000 °C in vacuum and then quickly transferred into the cell. The cell is connected to a temperature regulated platform through a $\frac{1}{4}$-in.-diam glass tube, which communicates with a gas supply. Temperatures above 30 K were determined by Pt resistance thermometry and below that by carbon thermometry. Temperature resolution of both thermometers was better than 1 mK throughout the experiment. A four-wire manufacturer calibrated germanium thermometer was used for temperature calibration.[37] The thermometer scales were adjusted to the published[32] bulk Ar and Ne triple points, 83.80 and 24.55 K, and located in the experiment by appropriate extrapolation of thick film triple-point melting peaks.[7] Thermal relaxation time τ_{int} within the cell is typically on the order of several seconds, while the external time τ_{ext} between the cell and its surroundings varies from about 45 min at 15 K to several hours at $T > 60$ K. A vapor pressure isotherm of Ar at 78 K clearly shows steps associated with the formation of the first three layers. Using the "point-*B*" method and average Ar molecular area 11.5 Å^2 given by Stoltenberg and Vilches,[38] we obtain approximately 280 m^2 of total adsorption area, and 88.5 cm^3 at standard temperature and pressure (STP) capacity of the first solid layer of Ar. According to the ratio of bulk (111) plane areal densities of Ar and Ne, the first layer solid completion for Ne is approximately at 133 cm^3 (STP). Throughout this paper we will specify film thickness L in terms of the number of layers, assuming that a complete layer of Ar contains 88.5 cm^3 (STP), and a complete layer of Ne contains 133 cm^3 (STP). These values neglect the compressibility and thermal expansion of the film. The errors are unimportant in the analysis of thin films at relatively low temperature, but as discussed in Secs. III and IV, they may become significant in the interpretation of phenomena in thick films at higher temperature, where the layers become poorly defined.

We studied 16 Ar films, with thickness range $1.4 < L < 40$, and 24 Ne films, with thickness range $1.2 < L < 24$. The Ar and Ne supplies were purchased as high-purity research grade gases, and were purified through a liquid-nitrogen trap before admission into the cell. The pressure in the gas handling system was monitored by a 1000-Torr capacitance manometer, with reading precision of 0.01 Torr. Each film was annealed by warming well above T_t, then slowly cooled, at a rate typically 1.0 K per hour. The heat-capacity measurements were made with a semiautomatic data acquisition and reduction system.[36] Typical heating pulses produced temperature rises of 0.05–0.15 K in Ne films and 0.15–0.25 K in Ar. Each data point was obtained by a least-squares fit to the slow thermal drift of the sample after the heating pulse. An initial transient immediately following the heating pulse was excluded from the fit, to allow internal equilibrium to be reestablished. Before each heating pulse the system remained undisturbed for 10–15 min to ensure equilibrium between film and vapor. A direct measurement of the vapor pressure relaxation time showed it to be less than 1 min when the pressure was above a few Torr.

It was important to ensure that the films were uniform in thickness throughout the experimental range. We found no indications of bulk nucleation in the Ar vapor pressures and heat capacities, which agrees with the behavior of Ar/graphite observed at lower temperature.[39] We were particularly careful to observe the Ne films for evidence of bulk formation, in view of the clustering observed at low temperature.[39] In order to monitor the Ne, we made extensive vapor pressure measurements of four of the thickest films. Figure 1 shows comparisons of these vapor pressures over the experimental temperature range, and illustrates significant variations with thickness for all films with $L < 17$. Since their vapor pressures are appreciably below that of the $L = 24$ film, we conclude that Ne can form at least about 17 layers at $T \geq 20$ K. This thickness greatly exceeds the maximum two layers reported for Ne on graphite at low temperature,[39] but seems consistent with the larger thicknesses observed by Hanono, *et al.*[40] at $T > 13.5$ K and with the increases due to triple-point wetting[2] or with a wetting transition at lower temperature.

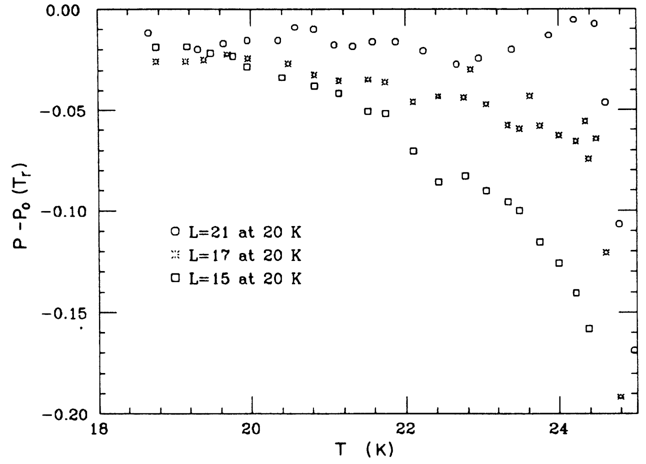

FIG. 1. Evidence for the absence of bulk nucleation in the Ne films at the experimental temperatures and coverages. The vapor pressures P of films of thickness $L = 15$ and 17 layers are lower than that of a sample of $L = 21$, and therefore of bulk P_0.

The heat-capacity measurements were taken nonisosterically; vapor desorption is appreciable, especially in thick films. The desorption correction to the heat capacity was calculated by the formula[41]

$$C_{\text{des}} = (q_{\text{st}} - k_B T)(dN/dT)_{\text{eq}} , \tag{1}$$

where q_{st} is the isosteric heat and assumed to be equal to the bulk value throughout. In order to determine the actual coverage N, we need to know the void space inside the cell and the vapor pressure. This was determined by volumetric measurements with He gas over a range of cell temperatures, which enabled us to estimate the effective volume in the filling line as well as the cell proper.

The vapor pressures of the Ar and Ne multilayer films were assumed to follow the Frenkel-Halsey-Hill (FHH) relation[41]

$$P = P_0 e^{-\alpha / k_B T L^3 \sigma^3} , \tag{2}$$

where σ is the atomic diameter and P_0 is the bulk vapor pressure. The values of α were determined from the measured vapor pressures of Ar and Ne films on graphite from one to three layers.[40,42] We believe that the desorption corrections are reliable for the thick films, but some indications of overcorrection and undercorrection are seen at thicknesses $L \leq 4$, where the variation of the isosteric heat and the deviation from the FHH relation become appreciable.

III. EXPERIMENTAL RESULTS

Figure 2 displays all locations of heat-capacity anomalies in Ar and Ne films found in this study, plotted

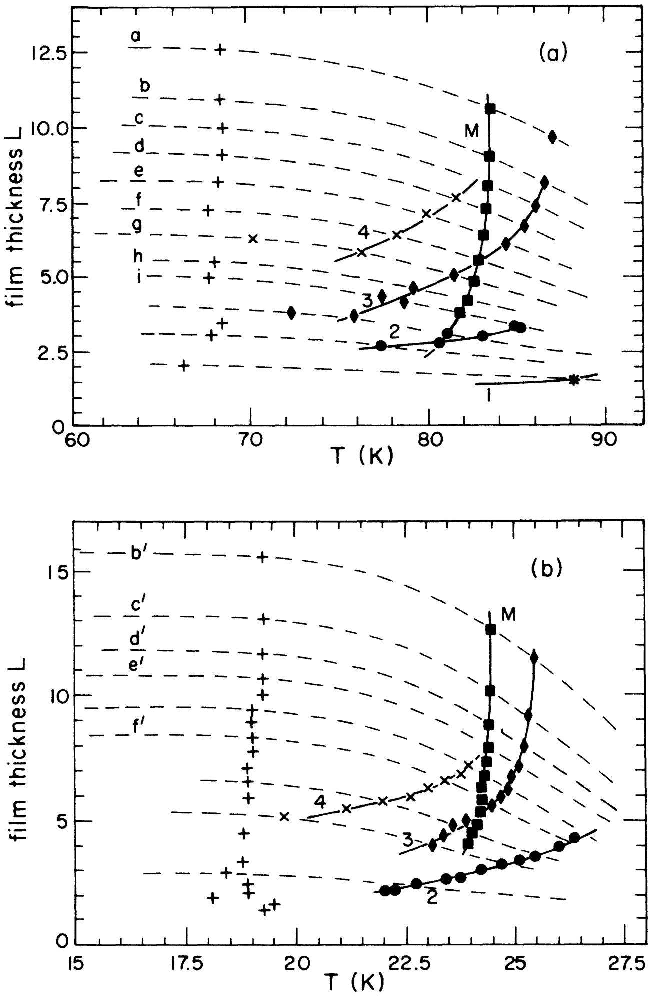

FIG. 2. The locations of heat-capacity anomalies and typical experimental paths of (a) Ar and (b) Ne films. The experiments were carried out in closed-cell geometry. The dashed lines are L-T trajectories calculated for desorption; lower case letters identify the film samples, listed in Table I. Different symbols classify the several types of anomalies which are related by shape, magnitude, and proximity. The symbols + are due to order-disorder transitions at the film-vapor interface. The series labeled (1), (2), (3) and (4) is due to the formation of the first four solid layers next to the substrate. The points labeled (M) leading up toward the triple-point temperature T_t are the locations of the surface melting peaks.

as film thickness versus temperature (see also Table I). The peaks trace out similar lines in the two systems. Figures 3(a), 3(b), and 4 show some typical heat-capacity data taken along the paths specified in Fig. 2. The data show many thickness-dependent features, particularly complex in the thinner films.

The most prominent features in both systems are the strong peaks close to the bulk triple-point temperatures. In the case of Ar, these peaks form a series extending from thickness $L \sim 3.5$ to the maximum $L = 40$. In Ne, the peak originates at about the same minimum thickness and extends to the maximum $L = 24$. The peaks have gradual precursors starting several degrees below T_t.

TABLE I. List of experimental film thicknesses. The calculated number of layers of argon and neon adsorbed at the bulk triple points.

Argon		Neon	
(a)	10.4	(a')	23.9
(b)	8.8	(b')	12.5
(c)	7.9	(c')	10.1
(d)	7.1	(d')	8.7
(e)	6.3	(e')	7.8
(f)	5.4	(f')	5.7
(g)	4.7		
(h)	4.1		
(i)	3.6		

The shape of the peaks in thick films shows a slight asymmetry, being steeper at $T > T_p$. The peak heights grow and the peak temperatures T_p gradually approach T_t from below as film thickness increases. Figure 5 shows the peaks of $L = 40$ Ar film and $L = 24$ Ne film, both of which are impressively high and narrow, but have the same type of asymmetry seen at lower coverage. The peaks are evidently associated with melting, and they tend toward a normal first-order triple-point transition of bulk material as $L \rightarrow \infty$.

Both Ar and Ne show small anomalies at about 80% of the triple-point temperatures: in Ar the anomalies are at $T \sim 68$ K, and in Ne at $T \sim 19$ K (shown in Figs. 2–4). These temperatures are very close to the third layer critical temperatures determined by vapor pressure isotherm measurements in each system.[40,42] Several heat-capacity scans in the second layer of Ne reveal a critical temperature at about 19.5 K, consistent with the isotherm results. At thicknesses $L < 6$, the peak shape and the peak temperature are quite sensitive to coverage; at some thicknesses the peak becomes fairly sharp. The anomalies tend asymptotically to higher temperatures as film thickness increases. At $L > 8$ the peak shape and magnitude become independent of further thickness increases. The anomalies in the thinner films are associated with layering transitions, and they evolve with thickness to a roughening transition.

Figures 3 and 4 show small cusp-shaped peaks at temperatures above the main melting peaks in both systems. We identify them as due to the melting of a layer near the substrate, the melting temperature being raised above T_t by the compression due to substrate attraction and interactions with higher layers.

The individual regions are analyzed in detail in the next section.

IV. ANALYSIS

Distinct two-dimensional phases are observed in a large number of adsorbed monolayer systems. With increasing coverage at low temperature, the first layer completes as a dense solid, and a second layer begins to form. The film may then undergo a sequence of pronounced

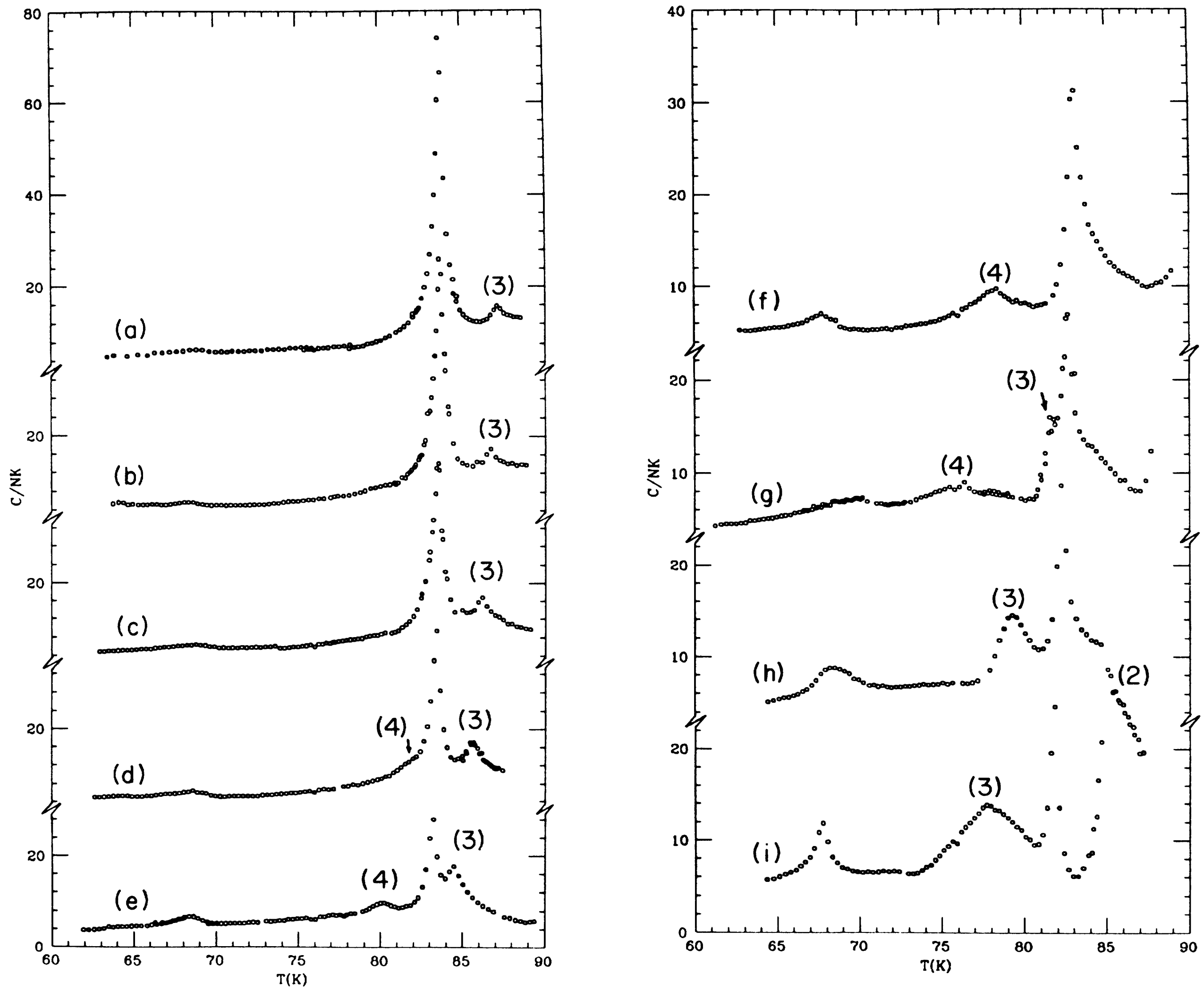

FIG. 3. (a) Specific heat of Ar/graphite, corrected for desorption. Letters refer to the film samples listed in Table I. The locations of the anomalies labeled (3) and (4) are shown in Fig. 2 and discussed in the text. (b) Specific heat of thin Ar/graphite films, corrected for desorption. Letters refer to the film samples listed in Table I. The locations of the anomalies labeled (2), (3), and (4) are shown in Fig. 2 and discussed in the text.

changes at thicknesses of two, three, or more layers.[24,25,43–48] The succession leads one to describe the features as if belonging to phases of the top layer, although in a strict sense each phase consists of the full thickness of the film, since all layers participate in the transitions. Nevertheless, it is convenient to describe the phases as if they were restricted to a single layer, and we will adopt this abbreviated terminology in the rest of the paper.

A. Layering transitions

Figure 6 displays the locations of the heat-capacity peaks at $L < 5$, together with the phase boundaries known from previous studies.[33,34,40,42]. The series of loops in Ar at $T < 70$ K and in Ne at $T < 20$ K are due to discrete layer transitions. Each loop is the boundary of a partially complete top layer, where the film is composed of regions of thickness $L - 1$ coexisting with thickness L. In a sense, the top surface is a two-phase monolayer adsorbed on a relatively inert substrate of thickness $L - 1$. Each loop ends at a layer critical point $T_c(L)$, $n_c(L) = L + \frac{1}{2}$. Although the loops resemble the two-dimensional (2D) liquid-vapor coexistence regimes of the first layers, the top layer of a thicker film typically has only one condensed phase and hence no triple point, because the atoms tend to be adsorbed on the sites of the layers below, so that both dense and rarefied quasi-2D phases have the same symmetry. The critical point is a 2D Ising second-order transition,[18,19] with critical exponents $\beta = \frac{1}{8}$, $\alpha = 0$. Several experiments[22,44–48] have yielded critical exponents in good agreement with theory. If a heat-capacity path passes through the critical density n_c at T_c, it results in a sharp heat-capacity peak with the form $C \sim |\ln(t)|$, where $t = |(T - T_c)|/T_c$. On the other

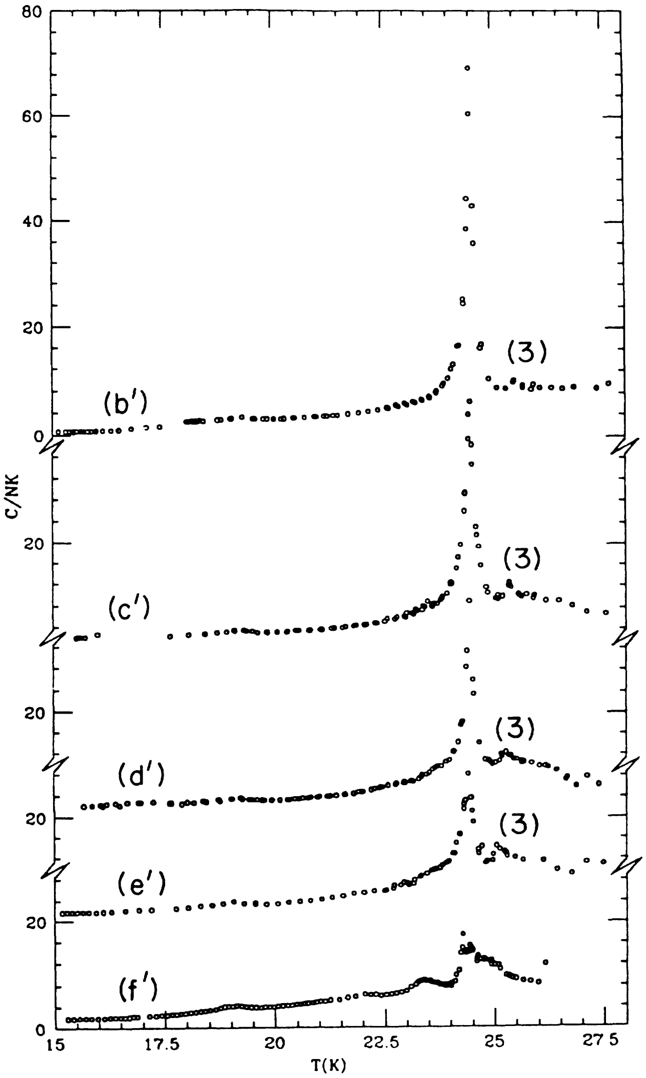

FIG. 4. Specific heat of Ne/graphite, corrected for desorption. Letters refer to the film samples listed in Table I. The locations of the anomalies labeled (4) are shown in Fig. 2 and discussed in the text.

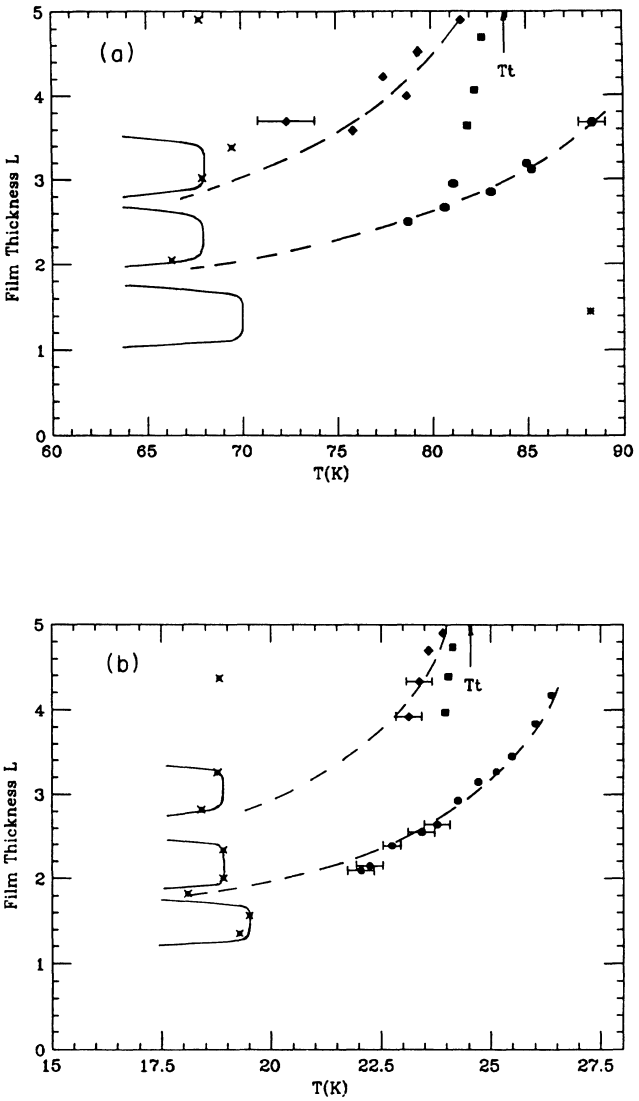

FIG. 6. Locations of heat-capacity anomalies found in thin films. The solid lines in the first three layers are based on the results in Refs. 33, 34, 41, and 42.

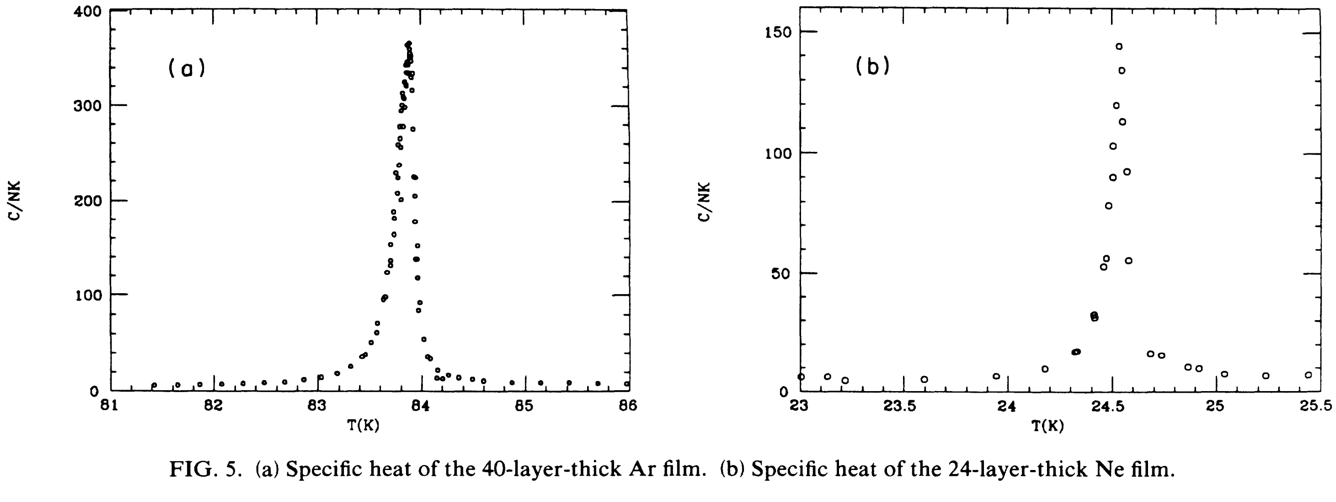

FIG. 5. (a) Specific heat of the 40-layer-thick Ar film. (b) Specific heat of the 24-layer-thick Ne film.

hand, if the density differs from n_c, the peak becomes weaker and asymmetric, off-critical density being equivalent to an external field in a magnetic system. If the heat-capacity path passes between two successive coexistence lines, there could be no heat-capacity anomaly at all.

In bilayers there can be an Ising transition between an adsorbed "fluid" and an ordered "solid", in that choice has been made between the two possible stackings. In trilayer and thicker films the situation is more complicated because the adsorption sites are not strictly equivalent, since the sites are distinguished by the presence or absence of an atom two layers deeper. But although the trilayer and thicker films cannot be described strictly by the two-sublattice model, the energy difference between the two types of sites is small, so that the model is not seriously compromised, and the experimental anomalies may be indistinguishable from Ising transitions.

Our results indicate that the experimental transitions are consistent with these considerations. For both Ar and Ne systems, the shape of the anomaly varies as the film thickness changes: at some coverages, it is a sharp cusp, but at others, quite rounded and weak. Figure 7 shows the cusp-shaped Ar peaks exhibiting their similarity to the logarithmic shape of 2D Ising transitions. We note that the estimated thicknesses are appreciably different from half integral layers, as called for in the model. The discrepancy can be ascribed to an appreciable density above the layer undergoing the transition. For example, the transition in the film of total thickness 4.9 layers is presumably due to ordering in the half-filled fifth layer, while an additional 0.4-layer equivalent provides a diffuse overlayer. In Fig. 7(b) we show several anomalies in Ne films at comparable coverages.

In the next section we discuss the evolution, with increasing thickness, of the discrete layer anomalies into surface roughening transitions.

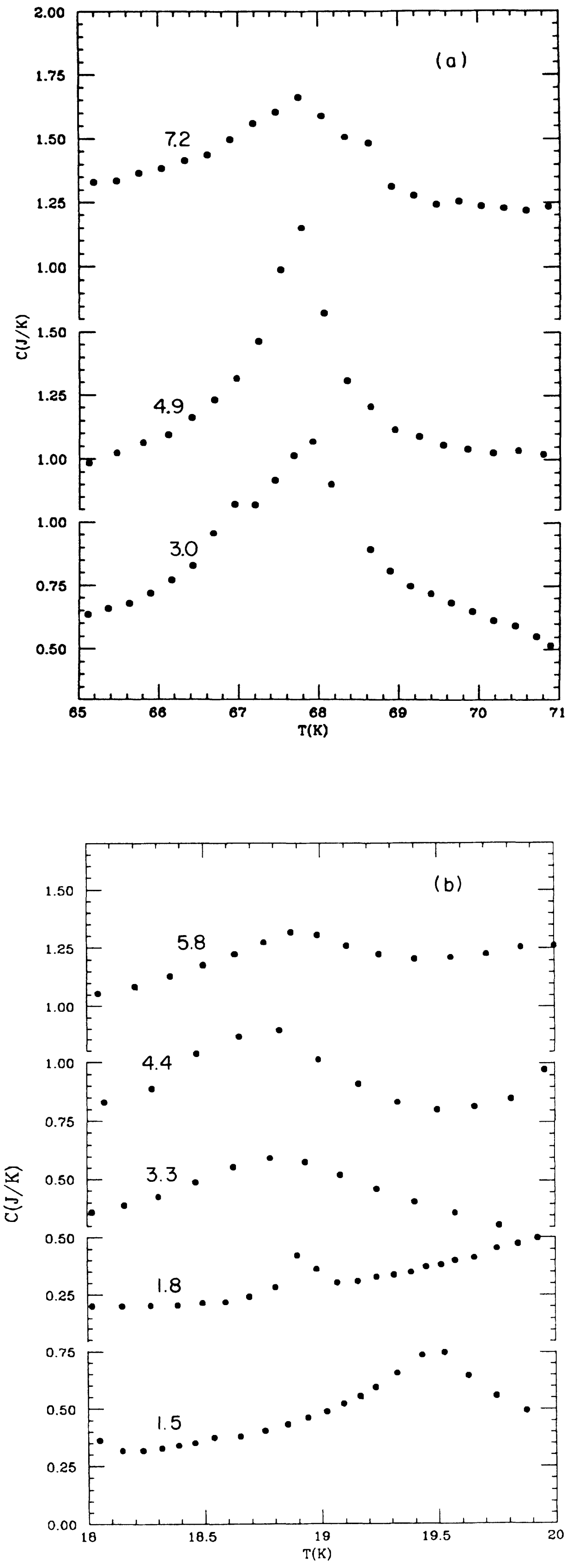

FIG. 7. The cusped anomalies due to layer critical transitions. (a) Ar; (b) Ne. The numbers are the estimated thicknesses at the temperatures of the anomalies.

B. Surface roughening in multilayer films

At the roughening transition of a semi-infinite crystal, a large number of thermally excited steps and kinks disorder the surface. Roughening is in the same universality class as the Kosterlitz-Thouless transition of the planar XY model.[11] The free-energy cost of creating a surface step vanishes in an essential singularity at the transition, hence there is no heat-capacity peak at T_R. However, a rounded specific-heat anomaly is expected to occur slightly below the transition temperature due to a rapid continuous change in the surface disorder.[11,20] Thermally excited steps and kinks can also occur in adsorbed multilayers, but their finite thickness limits the depth of the steps and the substrate field imposes an additional cost for step creation. If these limitations are sufficiently severe, the thickness disorder will involve only two distinct heights, so that the film is describable in terms of a two-state model. As film thickness increases, steps and kinks may be excited in several layers simultaneously, and the discrete layer transitions evolve to a roughening transition of the entire film. The evolution from layer transitions to roughening has been examined theoretically

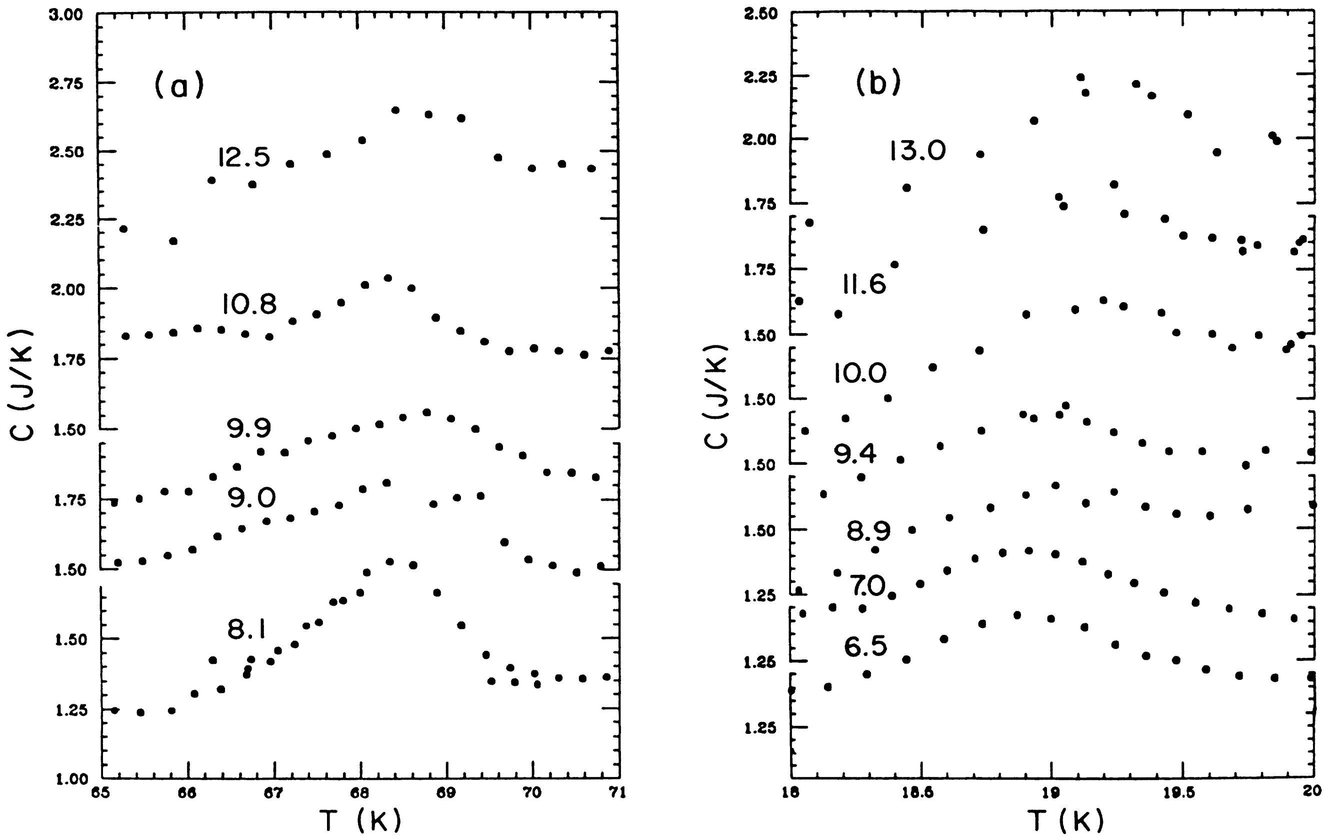

FIG. 8. The rounded, "roughening" anomalies in films thicker than those portrayed in Fig. 7. The numbers are the estimated thicknesses at the temperatures of the anomalies.

by Huse and by Nightingale, Saam, and Schick,[21] who predict that the layer critical temperature increases with thickness as $T_R - T_c(L) \sim 1/\ln^2(L)$.

Our results are consistent with predictions. The transition in a 7.2-layer Ar film shows the cusped shape of the 2D Ising model, therefore the transitions at this thickness are evidently still essentially restricted to a single layer, presumably the half-filled sixth. In Fig. 8 we show the heat capacities in the same regions of T, in thicker films. The anomalies are all rather broad and rounded, with no repetitions of the sharp cusp seen in thinner films, although it is possible that the selection of experimental coverage might have skipped over a sharp transition at a somewhat higher coverage. In Fig. 9 we plot the temperatures of the Ar and Ne specific-heat maxima at thicknesses between four and 14 layers, compared with the predicted temperature dependence. Our estimates of the peak temperatures are necessarily uncertain because the anomalies are so broad, so that the test is not stringent, but within the rather large uncertainty there is agreement with the theory.

The extrapolated roughening temperatures obtained from Fig. 9 are $T_R \sim 69.1$ for Ar and $T_R \sim 19.5$ for Ne, corresponding to $T_R \cong 0.8T_t$ for both types of film. The same relationship between roughening and melting temperatures of dense packed layers is obtained from computer simulations of molecular gases, equilibrium shapes of van der Waals solids, and vapor pressure isotherms of physisorbed gases. Computer simulation of a fcc Lennard-Jones crystal by Rosato, Ciccotti, and Pontikis[12] indicates a rapid increase of diffusional mobility, presumably due to roughening, at $T \sim 0.8T_t$ on the (110) facet. Experimental studies of equilibrium crystal shape of NH_4Cl by Jackson and Miller[16] and of Kr and Xe by

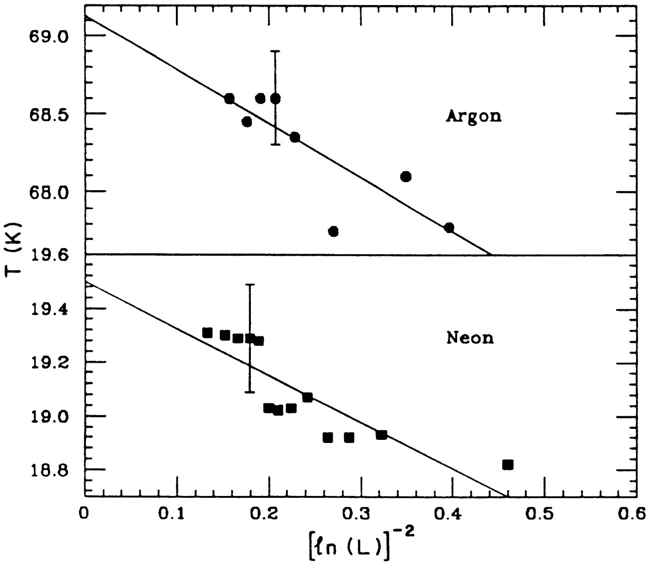

FIG. 9. The temperatures of the maxima of the "roughening" anomalies shown in Fig. 8. The straight lines are least-squares fits to the data.

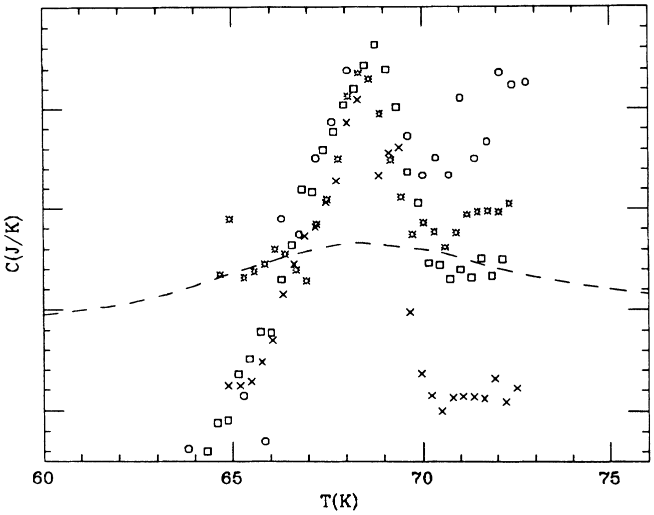

FIG. 10. Comparison of the "roughening" anomalies in four Ar films ($L = 12.5$, 10.8, 9.9, 9.0) with a Monte Carlo simulation (Ref. 20).

Maruyama[17] indicate roughening of (111) facets at $0.8T_t$. Vapor pressure isotherms of Ar films on Cl_2Cd by Larher[22] and of methane multilayers by Hamilton and Goodstein[24] yield approximately the same ratio.

In Fig. 10 we compare the peak shapes and widths in four thick Ar films with the results of a Monte Carlo study of the heat capacity in the neighborhood of a roughening transition.[20] We adjusted the step energy in the simulation to $60k_B$, so that the peak position would match our heat-capacity peaks. Figure 10 shows that the calculated specific-heat anomaly is considerably broader than the measured peak. The reasons are probably twofold. First, the simulation showed a trend of increasing sharpness of roughening peaks with crystal surface size.[20] The size used in the computation was 40×40, considerably smaller than the average coherence length of the foam graphite[49] On the other hand, roughening in a film of ten atomic layers is probably still truncated by the finite thickness.

We can estimate the surface step density in the roughened film from the specific-heat anomalies. The area under the roughening peaks corresponds to an entropy increase of about $0.25k_B$ per atom of surface layer. Assuming step heights of only one lattice spacing, the entropy implies an average step-step separation of five atomic spacings.

C. Melting of discrete layers

The series of melting anomalies, labeled (1), (2), (3), and (4) in Fig. 2, which extend upward in temperature from the regions of layer transitions, appears to be due to the melting of individual layers. This identification, originally made on the basis of a thermodynamic argument, is confirmed by direct observation via neutron spectroscopy.[35]

At the lowest coverage of Ar, $L \cong 1.4$, we observe a heat-capacity anomaly at $T = 88.2$ K (the location can be seen in Fig. 2). Since it falls on an extrapolation of the melting line of the first layer,[34] we so identify it here. A strong rise of the first layer melting temperature, to values in excess of T_t(3D), occurs in many physisorbed films. The rise is ascribed to the high areal density of the film, the compression being caused by a combination of the strong substrate field next to the wall, together with the "weight" of higher layers. Similar but weaker effects should occur in the second and higher layers, since the interaction falls off very quickly with separation.

The compression effect is treated in a simple model[50] which predicts the increase of melting temperature close to the substrate and the dependence on the total thickness of the film. The model is justified only in the limit of thick films, but it has been a useful guide for the interpretation of experiments on thin films of He, Ne, and H_2, by providing qualitative descriptions of the effects of solid-liquid stratification down to thicknesses as small as a few layers.[50-52] The theory treats the film as a continuum slab of bulk material, with finite compressibility and a first-order melting line. At temperatures not too far above the bulk triple point the film can become stratified, with a solid layer next to the substrate due to the compression by the field near the wall. The position of the solid-liquid interface L_s in a film of total thickness L is given as

$$L_s = (C_m + L^{-3})^{-1/3}; C_m = (\kappa\rho\alpha)^{-1}(1 - e^{\kappa(P_m - P_0)}) . \quad (3)$$

The compressibility and density of the bulk liquid are represented by κ and ρ;α represents the excess van der Waals interaction due to the substrate, $P_m(T)$ is the melting pressure, and $P_0(T)$ is the saturation vapor pressure. For the present study, we calculate the melting boundaries above T_t(3D) of Ar and Ne multilayers, according to the bulk melting lines $P_m(T)$ and liquid compressibilities,[32] and the interaction parameters with graphite.[53] Figure 11 displays the calculated melting temperatures $T_m(i,L)$ of the first three layers ($i = 1,2,3$) as a function of the total thickness L. The calculated curves show a very rapid rise with thickness of $T_m(1,L)$, to asymptotic limits 20% and 30% above T_t for the first layers of Ar and Ne, respectively. Comparable or stronger increases in first layer melting temperatures have been observed in methane[54] and hydrogen[44,55] films. The effect falls off rapidly with increasing distance from the substrate, but the melting of the second and third layers can still be distinguished from the triple-point anomaly. Figure 11 includes the positions of the experimental anomalies that lie above T_t, with tentative identifications as melting of particular layers. Although the measured peaks for both the second and third layers lie well above the calculated shifts, the trends with total thickness are consistent and in qualitative agreement. Conclusive confirmation is obtained by neutron scattering.[35] The shapes of the second and third layer melting peaks are intriguing. In Figs. 3(a) and 4 the third layer anomalies, which lie above the principal Ar and Ne melting peaks, are well shaped symmetric cusps. They resemble the layer critical point transitions (Sec. IV A), and they should be subject to the same

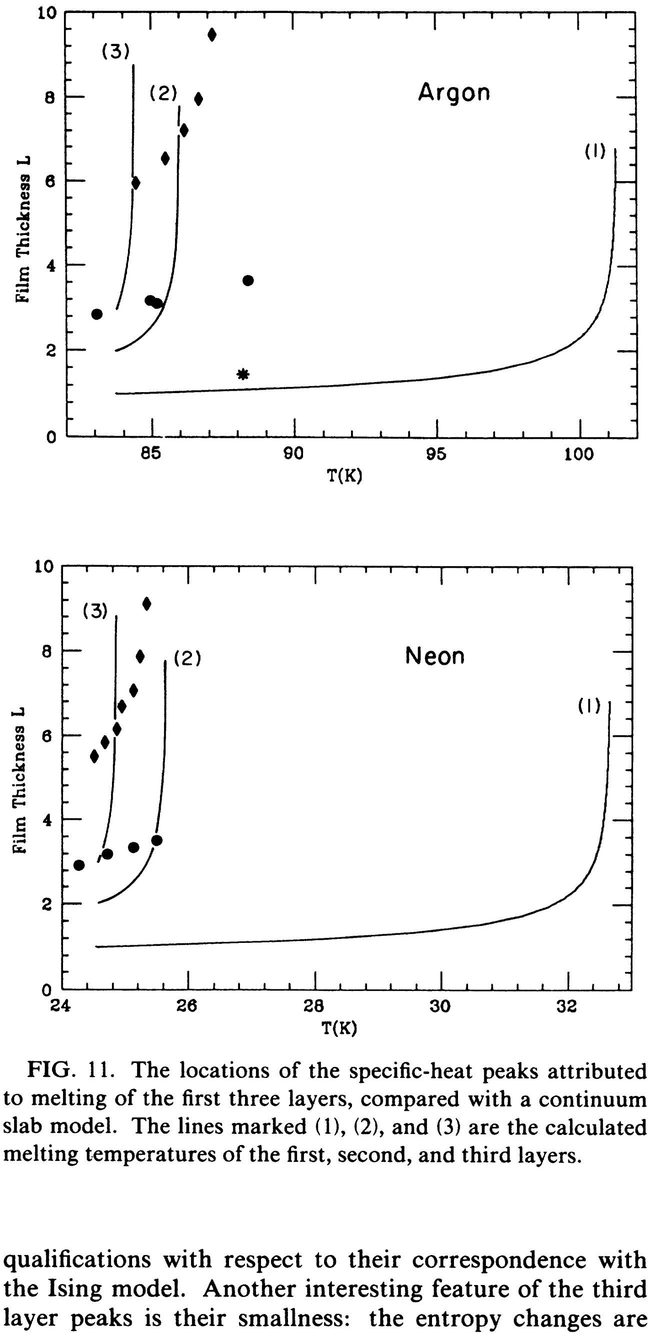

FIG. 11. The locations of the specific-heat peaks attributed to melting of the first three layers, compared with a continuum slab model. The lines marked (1), (2), and (3) are the calculated melting temperatures of the first, second, and third layers.

qualifications with respect to their correspondence with the Ising model. Another interesting feature of the third layer peaks is their smallness: the entropy changes are only about one-third of the melting entropy of a layer's population. The reduction is related to the finite width of the crystal-melt interface, which is discussed in Sec. IV E. The second layer melting anomalies, shown in Fig. 12, are markedly different from those of the third layer. The peaks are quite asymmetric, having steep risers on the low-T side, and much more gradual declines at high T. Their entropy changes are much greater than the bulk melting entropy of a layer's population. A strong enhancement of the melting heat-capacity anomalies in He films, occurring near monolayer completion, is quantitatively explained by Elgin and Goodstein[56] by the promotion to a higher layer of a fraction of the film due to its expansion on melting. We speculate that a similar process accounts for the strength and shape of the second layer Ar peaks shown in Fig. 12.

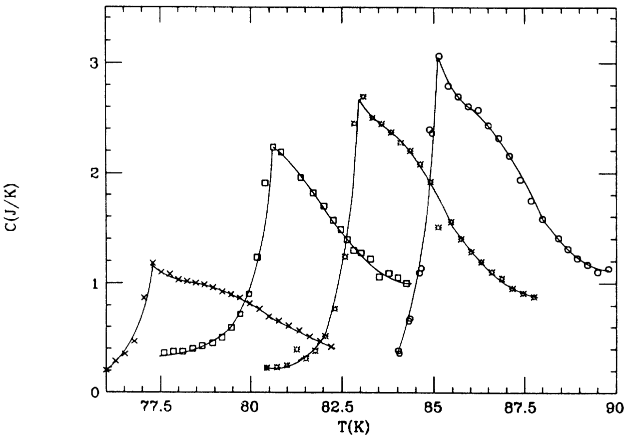

FIG. 12. The unusual heat-capacity peaks due to the melting of the second layer of Ar.

D. Surface melting in multilayer films

"Surface melting" means the appearance of a liquidlike disordered surface layer on a solid in equilibrium at temperatures below the bulk melting point. The motivation for the phenomenon is described by a thermodynamic argument,[3-7] summarized in the following paragraph.

If a solid is wetted by its melt liquid, the surface free energy at $T < T_t$ can be lowered by "premelting" a certain thickness of material, replacing the ionwetted solid-vapor coefficient $\gamma_{\rm sv}$ by the smaller sum $\gamma_{\rm lv}+\gamma_{\rm ls}$. The change $\delta F_{\rm surf}$ depends on the thickness L_l of the melted layer. The interfacial coefficients approach the γ's of bulk phases in the limit of very thick films but are functions of L_l at finite thickness, and this dependence introduces an effective attraction between the interfaces of the melted layer. In materials bound by molecular interatomic potentials varying as r^{-6} the interactions between plane interfaces vary as L_l^{-2}, so that the surface term is $\delta F_{\rm surf} = A(\gamma_{\rm lv}+\gamma_{\rm ls}-\gamma_{\rm sv})(1-{\rm const}\times L_l^{-2})$. For short-range interactions, $\delta F_{\rm surf} = A(\gamma_{\rm lv}+\gamma_{\rm ls}-\gamma_{\rm sv})(1-{\rm const}\times e^{-L_l/\xi})$. In addition to the change in surface free energy there is also an increase δF_m due to solid-liquid conversion, proportional to L_l. Minimizing $\delta F_{\rm surf}+\delta F_m$ with respect to L_l establishes the equilibrium thickness of liquid. Its variation with T arises from δF_m, which is zero at T_t and increases at lower T. Expanding δF_m in powers of $\Delta T = T_t - T$, the first-order results finds $L_l \sim (\Delta T)^{-1/3}$ for unretarded van der Waals forces and $L_l \sim |\ln(\Delta T)|$ for short-range interactions. The theory outlined neglects thermal fluctuations and assumes smooth interfaces, thus ignoring roughening. A justification for the approximation is given at the end of this section of the paper.

During melting the total signal consists of terms due to the liquid and solid and the progressive conversion from one to the other. In thick films, the phases are essentially homogeneous, except for portions close to the interface. Therefore the heat capacity at constant total N is the sum

$$C = Nc_s + N_l(c_l - c_s) + T\Delta s(dN_l/dT) + \delta C , \qquad (4)$$

where N_l is the population of melted atoms and c_l, c_s are the specific heats of uniform solid and liquid. δC is a lumped correction for desorption, finite thickness, and gradient effects. The terms due to premelting are distinguishable from the rest by their T dependence: N_l and dN_l/dT vary with ΔT, whereas all others are functions of T. The term in N_l diverges less strongly than dN_l/dT. With bulk values for the coefficients in Eq. (4), the term in N_l contributes no more than a few percent to the total. Hence to a fairly good approximation, the background-corrected heat capacity at $T < T_t$ is proportional to dN_l/dT.

We now compare the Ar and Ne heat-capacity data in the region of thick film melting peaks with this thermodynamic model of surface melting. Since the rises extend over only a few kelvins, the nonsingular background is approximated by a linear extrapolation from lower temperature, as $A + BT$. We show the background-corrected data of the thickest films as a function of ΔT in Fig. 13. The Ar data, for thicknesses between seven and ten layers, exhibit power-law behavior, $(\Delta T)^{-r}$, over about one decade: $0.0044 < \Delta T / T_t < 0.050$. There is no obvious trend of r with thickness, and the least-squares exponents are quite close: the average $r = 1.35 \pm 0.03$. Corrections due to finite heating intervals and the errors involved in "background" corrections are estimated to be no greater than 2%. Thus the empirical exponent of the Ar films in the 7–10 layer thickness range agrees with the theoretical value of $\frac{4}{3}$ for surface melting governed by nonretarded dispersion forces.

The Ne data were fitted in the same way over a consistent reduced temperature range extending over slightly more than one decade: $0.0055 < \Delta T / T_t < 0.075$. The Ne results differ from Ar, in that the empirical exponent r changes with the film thickness, progressing from about 1 at $L = 7$ to about $\frac{4}{3}$ at $L = 24$. The gradually changing exponent of Ne indicates a continuous evolution, from surface melting dominated by short-range interactions at small thickness, to melting dominated by long-range dispersion forces at large L_l. Recent studies of methane[8] and oxygen[9] films of one- to four-layer thickness have shown surface melting with logarithmic temperature dependence. Krim *et al.*[9] suggested that the apparent short-range interactions are an effect of the films' thinness, and our Ne results support the conjecture. In the next section we discuss the mechanism for the crossover and the reasons for the difference between the behavior of Ar and Ne.

The agreement between the experimental and theoretical exponents for the surface melting of thick films is at first sight surprising, in view of the fact that the theory assumes smooth interfaces, yet the temperature is well above the roughening temperature. However, the agreement is consistent with a prediction that mean-field theory should be applicable to this system.[5] The proof involves the concept of "upper marginal dimensionality" d^*, introduced in the renormalization-group analysis of phase transitions.[57] When the physical dimensionality d is larger than d^*, a system exhibits classical behavior, so that critical exponents have their mean-field values. Lipowsky and collaborators have shown that, in surface melting of a system governed by effective interfacial po-

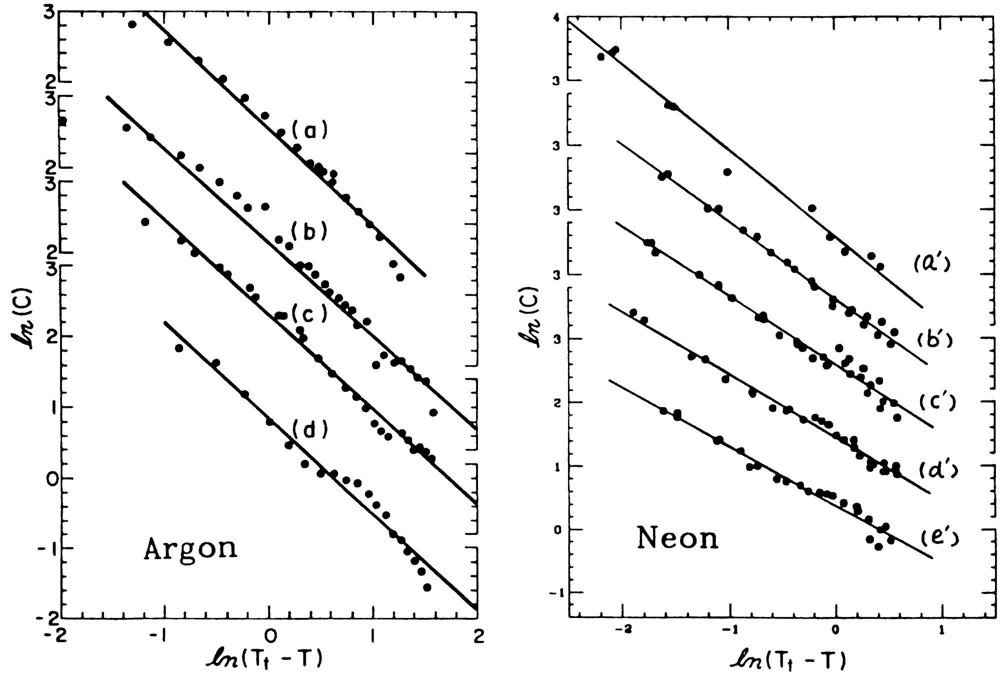

FIG. 13. Analysis of the precursors of the triple point, attributed to surface melting. Empirical power-law fits to the background-corrected heat capacities below T_t. Letters refer to the samples listed in Table I. The empirical exponents r for Ar are (a) 1.38, (b) 1.32, (c) 1.33, and (d) 1.35; For Ne (a') 1.34, (b') 1.20, (c') 1.08, (d') 0.98, and (e') 0.93.

tentials varying as L^{-p},

$$d^* = (3p+2)/(p+2) \ . \tag{5}$$

Since $p=2$ for the interfaces of van der Waals systems, $d^*=2$; thus the classical exponent is predicted. In contrast, $d^*=3$ in surface melting under short-range forces. In systems where $d=d^*$ there are logarithmic corrections near the transition, but perhaps they are not noticeable except in very precise measurements.

E. Crystal-melt interface profile

The basic theory described above assumes that the interface between solid and liquid is abrupt, the properties of the phases remaining unchanged up to the sharp boundary. The assumption is unrealistic, several theoretical and computer studies having shown that the solid-melt interface typically has a width of several atomic distances,[58,59] and indeed, the melt is more properly termed a "quasiliquid layer."[4,5] The solid also is modified in the neighborhood of the interface, so that there is a gradual change of solid crystalline order extending in both direction from the nominal boundary. The logarithmic growth observed in the surface melting of very thin films is caused by the short-range *effective* interactions associated with the finite width of the interface. These effective interactions arise from the short-range variation of the interfacial energy due to the intrusion of solidlike order into the liquid.[5] At distances much larger than the correlation length of the solid order parameter the growth of the melted layer settles into the dispersion force power law.

The fact that the Ne surface melting exponent exhibits a crossover to short-range behavior while Ar, in the same range of film thickness, does not, is presumably due to a shorter correlation length in Ar. We devised a method for measuring the correlation lengths, and found that the presumption is correct.

The gradual change from bulk solid to bulk liquid properties, combined with the control of thickness of the melted layer afforded by surface melting, provides the means for measuring the interface profile. The principle of the method can be applied to any measurement technique that can distinguish between liquid and solid properties. Of particular relevance here, one expects a gradual change in the entropy density $s(z)$ with distance z from the solid boundary. In the case of a liquid in contact with a smooth hard wall[59] the gradation is an exponential attenuation of solidlike properties with distance from the solid boundary:

$$s(z) = s_s + \Delta s(z) = s_s + \Delta s_m (1 - e^{-z/\xi'}) \ , \tag{6}$$

where Δs_m is the transition entropy density of bulk phases and ξ' is the coherence length of the solid order parameter. Equation (6) neglects the long-range effects of liquid-wall interactions, which in the case of dispersion forces introduce additional terms varying as z^{-3}. To apply this model to the film measurements we will neglect the diffuseness of the liquid-vapor interface, so that Eq. (6) with constant ξ' is assumed to extend throughout the liquid, to a sharp cutoff at the vapor boundary. The total transition entropy due to melting a finite thickness of film is an integral of $\Delta s(z)$; with L_0' as a fitting parameter for the number of unmelted layers, the total entropy of melting $L - L_0'$ layers is

$$\Delta S(L) = A\rho \, \Delta s_m [L - L_0' - \xi'(1 - e^{(L_0' - L)/\xi'})] \ , \tag{7}$$

where A is the area and ρ is the density of a liquid layer. L is the total film thickness.

At a crystal-melt interface the solid order parameter begins to change a short distance on the solid side of the boundary, so that the profile has a sigmoid shape in the central region, while the trend at greater distances on the liquid side is probably exponential. A simple model approximates the entire range by a hyperbolic tangent,

$$\Delta s(z) = \tfrac{1}{2} \Delta s_m [1 + \tanh(z/\xi)] \ . \tag{8}$$

At $z \gg \xi$, the entropy density approaches the bulk liquid value as $e^{-2z/\xi}$, so $\xi/2$ is the effective coherence length at large distances. 2ξ can be a gauge of the interface "width;" it is equal to the separation between the positions at which the parameters have undergone half of their total change. Integration for Δs requires an additional parameter, defined as L_0, to position the center of the interface relative to the substrate. The total transition entropy is

$$\Delta S(L) = A\rho \, \Delta s_m \left[L - L_0 + \tfrac{1}{2}\xi \ln \left[\frac{1 + e^{-2(L-L_0)/\xi}}{1 + e^{-2L_0/\xi}} \right] \right] \ . \tag{9}$$

Figure 14 displays the experimental $\Delta S(L)$ of Ne and Ar, obtained by integrating the area under the main melting peaks. The dashed lines represent the bulk entropy[32] for the same thickness range, i.e., how ΔS would vary with L if there were no interfacial effects. The measured $\Delta S(L)$ at large L tends to parallel the bulk lines but is shifted: the shift is approximately seven layers in Ne and 5.5 layers in Ar. The shifts are due to a combination of unmelted layers next to the substrate and crystal-melt interface effects. The data can be described quite well by both the exponential and hyperbolic tangent functions, with Δs_m being the bulk values and A the experimental substrate area. The figure shows the fitted hyperbolic tangent function; the best parameters are Ne: $\xi=3$, $L_0=6$, Ar: $\xi=1.9$, $L_0=5$. Standard deviations between the data and the fitted curves are 6%(Ne) and 7%(Ar). The optimum exponential function parameters are Ne: $\xi'=4.4$, $L_0'=2.5$; Ar: $\xi'=3.0$, $L_0'=2.5$, with standard deviation 8% for both systems, slightly greater than for the hyperbolic tangent function. The interface width, according to the hyperbolic tangent function, accordingly, is about six layers in Ne and four layers in Ar. The number of solid layers next to the substrate can also be obtained from the fitting parameters. In the hyperbolic tangent function fit, it is approximately equal to $L_0 - \xi$ and in the exponential function fit it is equal to L_0'. Thus according to this analysis there are two or three solid layers remaining unmelted at temperatures slightly above

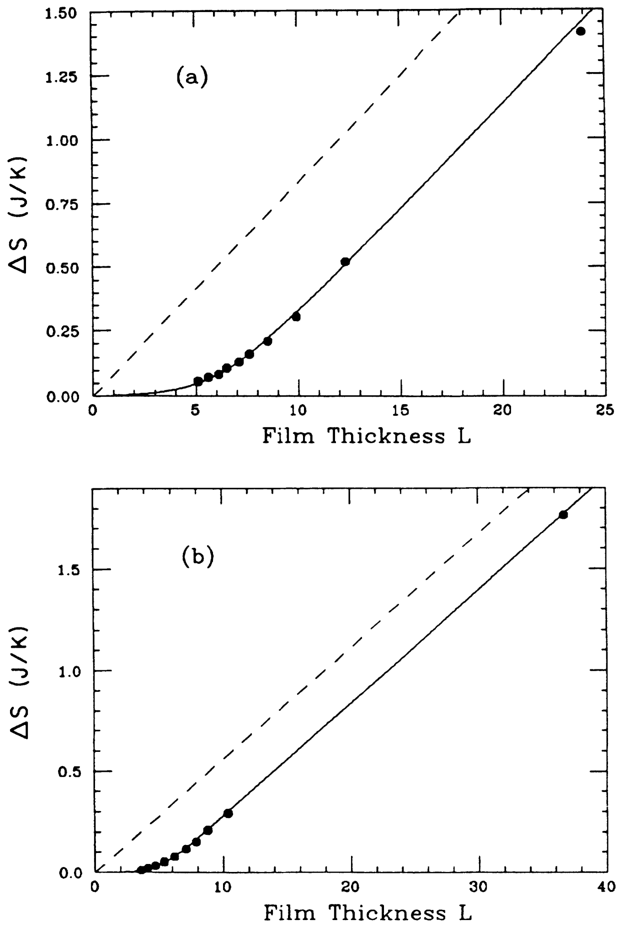

FIG. 14. Total entropy in the melting peaks of (a) Ne and (b) Ar films as functions of thickness. The dashed lines correspond to the empirical melting entropy of equivalent quantities of bulk material (Ref. 32), i.e., without surface corrections. The solid lines include calculated effects due to the finite width of the crystal-melt interface, showing the suppression of the total melting entropy due to the intrusion of solid order in the liquid adjacent to the solid boundary.

the main melting peak, agreeing with our estimates in Sec. IV C.

The experimental interface widths are comparable to theoretical estimates and computer simulations.[58,59] However, the difference between the Ne and Ar values is unexpected in view of the similarities of the two systems. The difference is well outside of statistical uncertainty and seems unrelated to the details of the assumed shape of the interface. However, we note that the compressibility of liquid Ne at its triple point is about twice that of Ar.[32] A simple argument based on the continuum model described in Sec. IV C predicts that the thickness of the liquid affected by the solid scales as $\kappa^{1/3}$. This model then predicts that the interface widths for Ar and Ne are in the ratio 1:1.3, in fair agreement with the ratio of measured coherence lengths.

The difference between the coherence lengths of Ar and Ne explains why crossover was seen in only the Ne samples. When an Ar film with total thickness $L \sim 7$ melts, the melt layer thickness is considerably larger than the crystal-melt interface width, while in a Ne film with about the same L the liquid layer thickness is comparable to the interface width and the system is dominated by effective short-range interfacial interactions.

The several features of surface melting in Ar, including the width of the crystal-melt interface, the crossover from logarithmic to power-law growth, and the thickness of unmelted layers above the triple point, are in close agreement with neutron scattering results.[35]

V. DISCUSSION

This study permits us to construct a common phase diagram for Ne and Ar on graphite, over a considerable portion of the range from monolayers to bulk coexistence. The similarities between the two systems are striking, and their differences are apparently only a matter of scale. In spite of the correspondences, however, the observations do not and cannot represent all combinations of adsorbates and substrates. Phase diagrams have been proposed for other systems[24,28,47] which have markedly different relationships between wetting, roughening, and layering phenomena. The differences result from variations in the several parameters, such as the strength of the substrate holding potential relative to the interactions between adsorbate atoms, and the degree of mismatch between adsorbate and substrate structures. Nevertheless, the Ne-Ar diagram shares several features that have been observed in other films. Figure 15 presents the common multilayer phase diagram with a summary of the conclusions obtained from the detailed analysis in Sec. IV. We first note the apparent similarity in the wetting behavior of the Ar and Ne: the experiments detected no evidence of incomplete wetting in either system. The apparent wetting of Ar is consistent with low-temperature observations of uniform films at least ten layers thick,[39] but the Ne result has to be attributed to a wetting transition at lower temperature or to triple-point wetting,[2] and that an extension of the study to lower temperature and/or higher coverage would discover bulk nucleation. But over the limited range of thickness and temperature in the study, both systems adsorbed as uniform films. Figures 15 shows a succession of layering transitions, extending to coexistence. A limited succession is seen in several adsorption systems, by vapor pressure, ellipsometry, and other techniques.[22,24,25,40,46] Finite experimental resolution restricts the number of distinct layers that can be detected, but the series is expected to continue *ad infinitum* to bulk in wetting systems at relatively low temperatures. Oliveira and Griffiths[18] obtained an infinite succession in a study of a lattice gas model of layering, and showed that near coexistence each first-order transition terminates at a layer critical point. The progression with L of $T_c(L)$ is predicted[21] to be a monotonic increase to the roughening transition temperature T_R, and as described in Sec. IV B, our results, for $L > 4$ layers, are consistent with theory.

The heat capacity indicates that several layers remain solid above the triple point if the vapor pressure is close to saturation, and this is confirmed by neutron scatter-

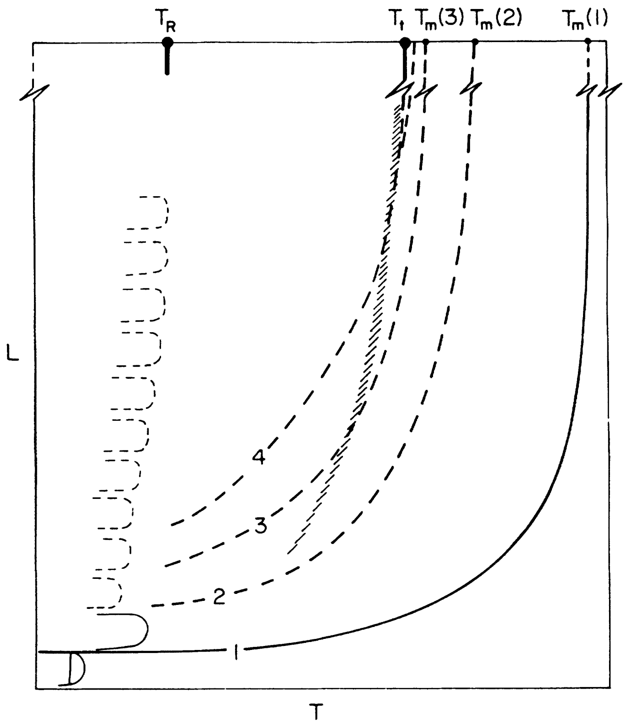

FIG. 15. Thickness-temperature diagram for Ar and Ne multilayers adsorbed on graphite. The succession of loops at low T are order-disorder transitions at the vapor interface, leading to a roughening transition at the surface of the bulk solid. The line labeled (1) marks the formation of the first solid monolayer. The series of lines (2), (3), and (4) show the ranges of L and T where the next three solid layers form. The hatched line leading down from the triple point marks the maximum rate of melting, near the highest temperature of surface melting. Solid lines represent boundaries between distinct thermodynamic phases; all others are gradual transformations, not true phase transitions.

ing.[35] The solidification is explained by the densification resulting from the substrate attraction combined with the weight of higher layers. An and Schick[29] find such behavior on the basis of a spin-1 model, and Krim and Dash[50] obtain similar results from a continuum slab model. In the spin model, the number of layers that remain solid in a thick film above T_t may be very large; according to the slab model nearly the entire film may be solid just above the triple point. Thus the melting temperature $T_m(L)$ approaches T_t from above as L becomes large.

The surface melting observations and their comparisons with theory are discussed in Sec. IV and will not be repeated here. We now discuss the relationships between the layer phenomena and bulk surface effects. The phase diagram shows how the individual layer transitions evolve to surface roughening and surface melting as the films become very thick. The evolution to roughening is the progression of layer critical points, now well established by many experiments and understood in detail by theoretical studies. The present results show how the melting of individual layers in a finite thickness film combine to become a continuous surface melting in thick films. At temperatures above T_R, the individuality of single layers is increasingly blurred in higher layers due to the rapid decrease of the substrate field; far from the wall, the distinctions become completely lost in the roughened film. The number of layers that can be distinguished above T_R depends on the relative importance of the substrate potential: in this study the limit for Ne and Ar seems to be four layers, but other probes and systems might yield other limits.

Roughening and surface melting, although they involve different forms of surface disorder, may have to be treated as more closely related than is usually assumed. In these materials surface melting involves roughened surfaces, so that the simple smooth interface model of surface melting is not strictly appropriate. However, as discussed earlier in the paper, the critical exponents for surface melting governed by dispersion forces are not affected by fluctuations. But other consequences of roughness are possible. The start of surface melting may take place at a lower temperature on a rough surface, the effective width of the crystal-melt interface will be greater if the crystal boundary is rough, and the roughness itself is likely to be increased when melting occurs.[60]

Finally, we point out that the basic idea for profiling the crystal-melt interface is adaptable to experimental probes other than calorimetry. The principle of the method is the control of the thickness of melt liquid that can be obtained through small temperature changes near T_t in a multilayer film undergoing surface melting. Ordinary adsorption techniques are the means for sensitive adjustment of the total film thickness; it is the total thickness that provides the fundamental scale of length.

ACKNOWLEDGMENTS

We thank M. Bienfait, M. den Nijs, D. L. Goodstein, R. E. Peierls, J. M. Phillips, J. Suzanne, L. B. Sorensen, E. K. Riedel, O. E. Vilches, and M. Wortis for numerous suggestions and stimulating conversations. Michael Elbaum's assistance in early stages of the project is gratefully acknowledged. We are particularly grateful to Michael Schick for his continuing interest and incisive advice, and we value our ongoing discussions as significant contributions to the success of the study. Research support was provided by the National Science Foundation, Grant Nos. DMR-81-16421, DMR-86-11466, and INT-86-12187.

[1] Recent reviews on wetting are given by D. E. Sullivan and M. M. Telo da Gama, in *Fluid Interfacial Phenomena*, edited by C. A. Croxton (Wiley, New York, 1986); S. Dietrich, in *Phase Transitions and Critical Phenomena*, edited by C. Domb and J. Lebowitz (Academic, London, 1988), Vol. 12.

[2] J. Krim, J. G. Dash, and J. Suzanne, Phys. Rev. Lett. **52**, 640 (1984); M. Drir and G. B. Hess, Phys. Rev. B **33**, 4758 (1986); A. D. Migone, J. G. Dash, M. Schick, and O. E. Vilches, *ibid.* **34**, 6322 (1986); A. D. Migone, A. Hofmann, J. G. Dash, and O. E. Vilches, *ibid.* **37**, 5440 (1988).

[3] J. K. Kristensen and R. M. J. Cotterill, Philos. Mag. **36**, 437 (1977).

[4] J. Q. Broughton and G. H. Gilmer, Acta Metall. **31**, 845 (1983); J. Chem. Phys. **79**, 5095 (1983); **79**, 5105 (1983); **79**, 5119 (1983); **84**, 5741 (1986); **84**, 5749 (1986); **84**, 5759 (1986); D. Nenow and A. Trayanov, J. Cryst. Growth **79**, 801 (1986); S. Valkealahti and R. M. Nieminen, Phys. Scr. **36**, 646 (1987).

[5] R. Lipowsky, Phys. Rev. Lett. **49**, 1575 (1982); R. Lipowsky and W. Speth, Phys. Rev. B **28**, 3983 (1983); D. M. Kroll, R. Lipowsky, and R. K. P. Zia, *ibid.* **32**, 1862 (1985).

[6] J. W. M. Frenken and J. F. van der Veen, Phys. Rev. Lett. **54**, 134 (1985); J. W. M. Frenken, P.M. Maree, and J. F. van der Veen, Phys. Rev. B **34**, 7506 (1986); B. Pluis, A. W. Denier van der Gon, J. W. M. Frenken, and J. F. van der Veen, Phys. Rev. Lett. **59**, 2678 (1987).

[7] D. M. Zhu and J. G. Dash, Phys. Rev. Lett. **57**, 2959 (1986); **60**, 432 (1988).

[8] M. Bienfait, Europhys. Lett. **4**, 79 (1987).

[9] J. Krim, J. P. Coulomb, and J. Bouzidi, Phys. Rev. Lett. **58**, 583 (1987).

[10] A. Trayanov and E. Tosatti, Phys. Rev. Lett. **59**, 2207 (1987).

[11] J. D. Weeks, in *Ordering in Strongly Fluctuating Condensed Matter Systems*, edited by T. Riste (Reidel, Dordrecht, 1979), p. 293; J. P. van der Eerden, P. Bennema, and T. A. Cherepanova, in *Progress in Crystal Growth and Characterization*, edited by B. R. Pamplin (Pergamon, New York 1979), Vol. 3, p. 219; J. D. Weeks and G. H. Gilmer, Adv. Chem. Phys. **40**, 157 (1979).

[12] V. Rosato, G. Ciccotti, and V. Pontikis, Phys. Rev. B **33**, 1860 (1986).

[13] J. C. Heyraud and J. J. Metois, J. Cryst. Growth **50**, 571 (1980); Surf. Sci. **128**, 334 (1983).

[14] C. Rottman and M. Wortis, Phys. Rep. **103**, 59 (1984).

[15] S. G. Lipson, Contemp. Phys. **28**, 117 (1987).

[16] K. A. Jackson and C. E. Miller, J. Cryst. Growth **40**, 169 (1977).

[17] M. Maruyama, J. Cryst. Growth (to be published).

[18] M. J. Oliveira and R. B. Griffiths, Surf. Sci. **71**, 687 (1978).

[19] R. Pandit, M. Schick, and M. Wortis, Phys. Rev. B **26**, 5112 (1982).

[20] R. H. Swendsen, Phys. Rev. B **18**, 492 (1978); G. Jacucci and N. Quircke, Phys. Lett. **98A**, 269 (1983).

[21] D. A. Huse, Phys. Rev. B **30**, 1371 (1984); M. P. Nightingale, W. F. Saam, and M. Schick, *ibid.* **30**, 3830 (1984).

[22] Y. Larher and F. Millot, J. Phys. (Paris), Colloq. **38**, C4-189 (1977); Y. Larher, Mol. Phys. **38**, 789 (1979).

[23] W. F. Saam, Surf. Sci. **125**, 252 (1983).

[24] J. J. Hamilton and D. L. Goodstein, Phys. Rev. B **28**, 3838 (1983); D. L. Goodstein, J. J. Hamilton, M. J. Lysek, and G. Vidali, Surf. Sci. **148**, 187 (1984).

[25] S. Ramesh, Q. Zhang, G. Torzo, and J. Maynard, Phys. Rev. Lett. **52**, 2375 (1984).

[26] M. Den Nijs, E. K. Riedel, E. H. Conrad, and T. Engel, Phys. Rev. Lett. **55**, 1689 (1985); **56**, 4028(E) (1986); E. H. Conrad, R. Aten, D. Kaufman, L. Allen, T. Engel, M. den Nijs, and E. K. Riedel, J. Chem. Phys. **84**, 1015 (1986); **85**, 4756(E) (1986).

[27] J. Villain, D. R. Grempel, and J. Lapujoulade, J. Phys. F **15**, 809 (1985); J. Lapujoulade, Surf. Sci. **178**, 406 (1986).

[28] S. G. J. Mochrie, M. Sutton, R. J. Birgeneau, D. E. Moncton, and P. M. Horn, Phys. Rev. B **30**, 263 (1984); S. G. J. Mochrie, Phys. Rev. Lett. **59**, 304 (1987); G. A. Held, J. L. Jordan-Sweet, P. M. Horn, A. Mark, and R. J. Birgeneau, *ibid.* **59**, 2075 (1987); K. S. Liang, E. B. Sirota, K. L. D'Amico, G. J. Hughes, and S. K. Sinha, *ibid.* **59**, 2447 (1987).

[29] G. An and M. Schick, Phys. Rev. B **37**, 7534 (1988).

[30] J. G. Dash, in *Proceedings of the XIX Solvay Congress*, edited by F. W. DeWette (Springer-Verlag, Berlin, 1988).

[31] J. G. Dash, Phys. Today **38**, 26 (1985).

[32] R. K. Crawford, in *Rare Gas Solids*, edited by M. L. Klein and J. A. Venables (Academic, New York, 1977), Vol. 2.

[33] G. B. Huff and J. G. Dash, J. Low Temp. Phys. **24**, 155 (1976); R. E. Rapp, E. P. de Souza, and E. Lerner, Phys. Rev. B **24**, 2196 (1981).

[34] T. T. Chung, Surf. Sci. **87**, 348 (1979); A. D. Migone, Z. R. Li, and M. H. W. Chan. Phys. Rev. Lett. **53**, 810 (1984); J. P. McTague, J. Als-Nielsen, J. Bohr, and M. Nielsen, Phys. Rev. B **25**, 7765 (1982).

[35] J. M. Gay, J. Suzanne, H. J. Lauter, and J. G. Dash (private communcation).

[36] F. C. Motteler, Ph.D. thesis, University of Washington, 1986 (unpublished).

[37] CryoCal, Inc.

[38] J. Stoltenberg and O. E. Vilches, Phys. Rev. B **22**, 2920 (1980).

[39] M. Bienfait, J. L. Seguin, J. Suzanne, E. Lerner, J. Krim, and J. G. Dash, Phys. Rev. B **29**, 983 (1984).

[40] F. Hanono, C. E. N. Gatts, and E. Lerner, J. Low Temp Phys. **60**, 73 (1985); E. Lerner, F. Hanono, and C. E. W. Gatts, Surf. Sci. **160**, L524 (1985).

[41] J. G. Dash, *Films on Solid Surfaces* (Academic, New York, 1975).

[42] B. Gilquin, Ph.D. thesis, University of Nancy, 1979 (unpublished).

[43] S. E. Polanco and M. Bretz, Phys. Rev. B **17**, 151 (1978).

[44] J. Ma, T. A. Sullivan, O. E. Vilches, Jpn. J. Appl. Phys. **26-3**, 263 (1987).

[45] Q. M. Zhang, Y. P. Feng, H. K. Kim, and M. H. W. Chan, Phys. Rev. Lett. **57**, 1456 (1986); Phys. Rev. B **37**, 3511 (1988).

[46] H. S. Nham, M. Drir, and G. B. Hess, Phys. Rev. B **35**, 3675 (1987).

[47] Q. M. Zhang, H. K. Kim, and M. H. W. Chan, Phys. Rev. B **34**, 8050 (1986).

[48] M. H. W. Chan and Y. P. Feng, Bull. Am. Phys. Soc. **33**, 283 (1988).

[49] R. G. Birgeneau, P. A. Heiney, and J. P. Pelz, Physica B + C **109&110B**, 1785 (1982).

[50] J. Krim and J. G. Dash, Surf. Sci. **162**, 421 (1985).

[51] A. D. Migone, J. G. Dash, O. E. Vilches, and M. Schick, Phys. Rev. B **34**, 6322 (1986).

[52] A. D. Migone, A. Hofman, J. G. Dash, and O. E. Vilches, Phys. Rev. B **37**, 5440 (1988).

[53] J. Krim, Ph.D. thesis, University of Washington, 1984.

[54] J. P. Coulomb, M. Bienfait, and P. Thorel, J. Phys. (Paris) **42**, 293 (1981).

[55] H. Freimuth and H. Wiechert, Surf. Sci. **176**, 716 (1986).

[56] R. L. Elgin and D. L. Goodstein, Phys. Rev. A **9**, 2665 (1974).

[57] A. Aharony and B. Halperin, Phys. Rev. Lett. **35**, 1308 (1975); J. Als-Nielsen and R. J. Birgeneau, Am. J. Phys. **45**, 554

(1977).

[58] A. Bonissent, *Interfacial Aspects of Phase Transitions,* edited by B. Mutaftschiev (Reidel, Dordrecht, 1982); J. W. Broughton, A. Bonissent, and F. F. Abraham, J. Chem. Phys. **74**, 7029 (1981); W. H. Shih, Z. Q. Wang, X. C. Zeng, and D. Stroud, Phys. Rev. A **35**, 2611 (1987); W. A. Curtin, Phys. Rev. Lett. **59**, 1228 (1987).

[59] R. Evans, Adv. Phys. **28**, 143 (1979); P. Tarazona and L. Vicente, Mol. Phys. **56**, 557 (1985).

[60] K. Kariotis, H. Suhl, and B. Yang, Phys. Rev. B **32**, 4551 (1985).